Heterogeneous dynamics of the three-dimensional Coulomb glass out of equilibrium

Alejandro B. Kolton
Université de Genève, DPMC, 24 Quai Ernest Ansermet, CH-1211 Geneve 4, Switzerland

D. R. Grempel
CEA-Saclay, DSM/DRECAM/SPCSI, 91191 Gif-sur-Yvette Cedex, France

Daniel Domínguez
Centro Atómico Bariloche, 8400 San Carlos de Bariloche, Río Negro, Argentina
(Received 28 July 2004; published 25 January 2005)

The nonequilibrium relaxational properties of a three-dimensional Coulomb glass model are investigated by kinetic Monte Carlo simulations. Our results suggest a transition from stationary to nonstationary dynamics at the equilibrium glass transition temperature of the system. Below the transition the dynamic correlation functions lose time translation invariance and electron diffusion is anomalous. Two groups of carriers can be identified at each time scale: electrons whose motion is diffusive within a selected time window and electrons that during the same time interval remain confined in small regions in space. During the relaxation that follows a temperature quench an exchange of electrons between these two groups takes place and the nonequilibrium excess of diffusive electrons initially present decreases logarithmically with time as the system relaxes. This bimodal dynamical heterogeneity persists at higher temperatures when time translation invariance is restored and electron diffusion is normal. The occupancy of the two dynamical modes is then stationary and its temperature dependence reflects a crossover between a low-temperature regime with a high concentration of electrons forming fluctuating dipoles and a high-temperature regime in which the concentration of diffusive electrons is high.

DOI: 10.1103/PhysRevB.71.024206 PACS number(s): 71.55.Jv, 75.10.Nr, 72.20.−i

I. INTRODUCTION

Recent experimental studies of hopping conductance in Anderson insulators showed striking nonequilibrium effects that persist for long times at low temperature.[1–5] These results support early theoretical predictions of a low-temperature glassy phase in interacting disordered electron systems in the strongly localized limit.[6,7] In this regime the essential physics is well captured by the Coulomb glass model that describes a system of interacting electrons hopping between randomly distributed sites that correspond to the localization centers of the single-electron wave functions.[6–11]

Although Coulomb glass models have been extensively studied during the last 30 years and their equilibrium properties are by now fairly well understood,[6–12] much less is known about the properties of Coulomb glasses out of equilibrium.[13–16]

In Ref. 16 the off-equilibrium dynamics of the Coulomb glass was investigated by studying the scaling properties of the nonstationary correlation and response functions, a tool often used in the study of other glassy systems such as structural and spin glasses.[17–20]

It has recently been realized that further insights into the nature of the glassy phase can be gained from the analysis of dynamical heterogeneities.[21–23] This approach is particularly appealing in the context of Coulomb glasses since the low-temperature hopping conductance is dominated by the diffusion of carriers on a set of conducting percolation paths.[6,7] We expect interactions between the electrons to have strong effects on this type of motion since hops of individual carriers alter the effective random potential felt by the others and thus modify the structure of the percolating network. Fluctuation effects of this type were shown to lead to low-frequency $1/f$-like noise in the conductance of Coulomb glasses.[24,25]

In this paper we investigate the dynamical properties of the three-dimensional random-site Coulomb glass model by kinetic Monte Carlo simulation using a realistic microscopic dynamics that favors the emergence of local effective constraints in the kinetics. In our simulations the system is initially quenched from infinite temperature to a working temperature T and its evolution in time is characterized for different values of T through the time dependence of the relevant correlation functions.

One of our main observations is the appearance of a dynamical crossover from equilibrium dynamics to slow nonequilibrium dynamics at a temperature $T_g \sim T_c$, where T_c is the equilibrium freezing transition temperature of the model.[11] This crossover takes place even for relatively small system sizes and occurs at the temperature at which the equilibration time of the finite sample becomes much longer than the time scale of the simulation. In this regime the time-dependent correlation functions exhibit slow relaxation and have aging properties. We found that the dynamics of the Coulomb glass is heterogeneous as observed in other glassy systems.[21,22] Heterogeneities can be characterized by examination of the evolution of diffusion fronts. A statistical analysis of the electron trajectories over a fixed time window shows that most carriers belong to one or the other of two groups. The first group is that of those electrons that diffused away from their initial position during the chosen time inter-

val. The second group is that of the electrons that remained confined in relatively small regions in space during that time. An exchange of electrons between these two dynamical modes takes place as the system relaxes after a temperature quench. In the aging regime this exchange is very slow and the nonequilibrium excess of electrons with metallic hopping present in the system right after the quench decreases logarithmically with time. In this temperature range the diffusion is anomalous. We found that the mean squared displacement $\langle \Delta x^2(t) \rangle \sim t^{\eta}$ where the exponent is $\eta < 1$ and depends on the age of the system. In the equilibrium regime time translation invariance is recovered and we observe normal diffusion. However, the bimodal dynamical heterogeneity still persists. The occupancy of the two dynamical modes is stationary and its temperature dependence reflects a crossover from a low-temperature regime with a high concentration of electrons forming fluctuating dipoles to a high-temperature regime in which the concentration of diffusive electrons is high.

The paper is organized as follows. Section II contains a description of the model and of our numerical method. In Sec. III we discuss the properties of the local-density autocorrelation function in and out of equilibrium. Section IV is devoted to the analysis of electron diffusion in the system. In Sec. V we study the statistical properties of the diffusion fronts and show that they provide evidence for the existence of heterogeneous transport in the system. Finally, we summarize the conclusions of our study in Sec. VI.

II. THE MODEL

The Hamiltonian of the classical three-dimensional Coulomb glass is[7]

$$H = \sum_i n_i \varphi_i + \frac{e^2}{2\kappa} \sum_{i \neq j} \frac{(n_i - K)(n_j - K)}{|\mathbf{R}_i - \mathbf{R}_j|}, \tag{1}$$

where $\mathbf{R}_i$ denotes the center of localization of a single-particle localized electronic state, φ_i the energy of the state, and e and κ are the electron charge and the medium's dielectric constant, respectively. Strong on-site correlations limit the occupancy of the electronic states to $n_i = 0, 1$. Charge neutrality is assured by a uniform compensating positive charge density $K = (1/N)\Sigma_i n_i$.

The positions $\mathbf{R_i}$ of the localized states and their energies φ_i are both random variables. However, it is common practice to study two complementary simplified versions of the model. These are referred to as the lattice model and the random site model, respectively, in Ref. 15. In the lattice model the sites are assumed to lie on a regular cubic lattice and only the randomness in the energies φ_i is taken into consideration. Conversely, in the random site model[10,11] only the positional disorder is taken into account and $\varphi_i = 0$. It is standard practice to concentrate on the particle-hole symmetric case $K = 1/2$ for which the analysis of the results is simpler.

While it has been established that the three-dimensional random-site model has an equilibrium glass transition at low temperature[11] it is not yet clear whether this is also the case for the lattice model.[12,26] Therefore, we shall only discuss the dynamics of the random-site model in this paper.

To model the dynamics of the system we let it evolve through sequential single-electron hops from occupied sites a to empty sites b. The transition rate, which mimics phonon assisted processes, is

$$\Gamma_{a \to b} = \tau_0^{-1} e^{-2R_{ab}/\xi} \min[1, e^{-\Delta E_{ab}/T}], \tag{2}$$

where τ_0 is a microscopic time, ξ is the spatial extension of the localized wave functions, and $R_{ab} \equiv |\mathbf{R}_a - \mathbf{R}_b|$. ΔE_{ab}, the total energy difference in the transition, is given by

$$\Delta E_{ab} = \epsilon_b - \epsilon_a - \frac{e^2}{\kappa R_{ab}},$$

$$\epsilon_a = \frac{e^2}{\kappa} \sum_{b \neq a} \frac{\delta n_b}{R_{ab}}, \tag{3}$$

$\delta n_i \equiv n_i - K$.

The first factor in Eq. (2) reflects the exponential decay of the electron-phonon matrix element between two electronic wave functions centered at positions $\mathbf{R}_a$ and $\mathbf{R}_b$. The second factor is the thermal part of the transition probability. In Monte Carlo simulations performed by other authors the transition probability is taken independent of the distance R_{ab} [the first exponential in the equivalent of Eq. (2) is absent].[9,11] This type of nonlocal dynamics, convenient for rapid equilibration, may not be appropriate for the study of off-equilibrium relaxation. With the local dynamics of Eq. (2) electron hops that decrease the energy are essentially restricted to a region whose linear size is the localization length ξ. This introduces dynamic constraints that contribute to make the relaxation out of an excited configuration slower.

In our simulations we take the mean distance between sites a_0 as the unit of length, the Coulomb energy $E_C = e^2/(\kappa a_0)$ as the unit of energy, and we choose for convenience $\xi = a_0$.

We simulated systems of $N = L^3$ sites and $M = N/2$ electrons for samples with $L = 6, 8$, and 10 in the temperature range $0.01 \leqslant T \leqslant 0.1$. The localization centers are distributed randomly and uniformly inside a computational cubic box of side L and we take periodic boundary conditions in all directions. To simulate a quench from high temperature we start from a random electron configuration at $t = 0$ and let the system freely evolve with the dynamics (2) at the working temperature T. The elementary Monte Carlo move consists of an attempt to move an electron from a randomly chosen occupied site a to an empty site b. Once a is chosen, the destination site b is chosen randomly using the probability distribution of the hoppings, $P(R_{ab}) \propto \exp(-2R_{ab})$. A cutoff at $R_{ab} = L/2$ is imposed by our use of periodic boundary conditions and restricts us to a range of temperatures for which hops at distances $R_{ab} \sim L$ can be neglected. The probability of acceptance of the move is the thermal factor in Eq. (2). If the hop is accepted, the vector displacement of the hopping electron $\delta \mathbf{r}$ is defined as the vector going from site a to the closest periodic image of site b. A Monte Carlo step (MCS) consists of N hopping attempts. Our runs were typically 2×10^6 MCS long. Physical quantities were monitored as a function of time for each sample and the results were averaged over

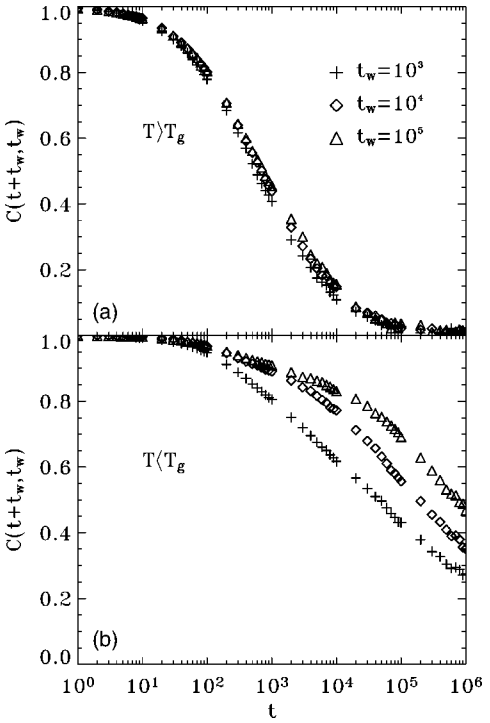

FIG. 1. Two-time charge autocorrelation functions for $T=0.07$ (a) and $T=0.03$ (b). Aging effects (loss of time translation invariance) become appreciable below the crossover temperature $T_g \approx 0.05$.

between 150 and 600 realizations of the disorder and initial conditions, depending on the system size and temperature.

III. THE LOCAL DENSITY AUTOCORRELATION FUNCTION

The two-time charge autocorrelation function is[16]

$$C(t+t_w,t_w)=\frac{2}{M}\sum_i \langle \delta n_i(t+t_w)\,\delta n_i(t_w)\rangle, \tag{4}$$

where the brackets denote the average over configurational disorder, initial conditions, and thermal noise, and the waiting time t_w is the time elapsed since the quench from infinite temperature.

The function $C(t+t_w,t_w)$ is the overlap of the charge configurations at times $t+t_w$ and t_w. If t_w is larger than the equilibration time $\tau_{\rm eq}$ the state of the system is time-translational invariant and the correlation function depends only on the time difference t. Otherwise, C depends on both t and t_w.

We describe in the following results for a system of linear size $L=10$. Figure 1 displays $C(t+t_w,t_w)$ versus t for three waiting times, $t_w=10^3, 10^4$, and 10^5, and two representative cases; $T=0.07$ [Fig. 1(a)] and $T=0.03$ [Fig. 1(b)]. We observe that in the first case $C(t+t_w,t_w)\approx C(t)$, i.e., the system is time-translational invariant. This means that equilibrium was reached within a time shorter than the shortest of the waiting times considered, $\tau_{eq}(T)<10^3$. $C(t)$ is thus the equilibrium relaxation function. In the second case, however, time translation invariance is lost and $C(t+t_w,t_w)$ depends on both time arguments, a phenomenon known as aging. The system was thus unable to equilibrate within the time scale of the simulation. Note that for each value of t_w the relaxation is very slow (roughly logarithmic) and becomes slower with increasing t_w.

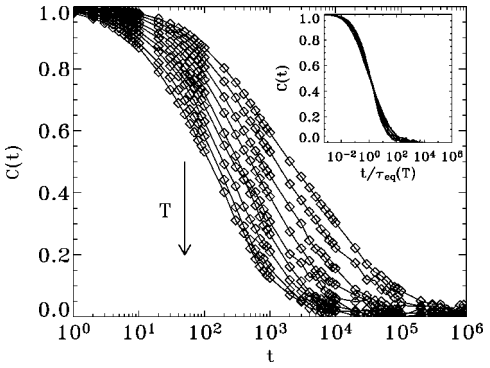

FIG. 2. The charge autocorrelation function at equilibrium for $T>T_g$. The curves correspond to $T=0.10$, 0.095, 0.09, 0.085, 0.080, 0.075, 0.070, 0.065, 0.060, 0.055, and 0.050 from bottom to top. The inset shows the same data but represented as a function of the rescaled time $t/\tau_{eq}(T)$, with $\tau_{eq}(T)=\exp(0.45/T)$.

We found that nonequilibrium relaxation appears below a dynamic crossover temperature $T_g \sim 0.05$. The value of T_g is remarkably close to the equilibrium transition temperature of the random-site model $T_c=0.043$ determined in Ref. 11.

Further insights into the properties of the correlation functions can be gained by performing a scaling analysis of the data. We discuss separately the cases of high and low temperatures.

A. $T>T_g$

In this temperature region the system reaches equilibrium within the simulation time. In Fig. 2 we show the equilibrium correlation function $C(t)$ obtained for several temperatures in the range $0.05\leqslant T\leqslant 0.1$. As shown in the inset to Fig. 2, the curves for the various temperatures collapse rather well into a single master curve when $C(t)$ is represented as a function of the scaled variable $t/\tau_{eq}(T)$, where $\tau_{eq}(T)=\exp(T_0/T)$ with $T_0\sim 0.45$. The equilibrium relaxation time thus obeys an Arrhenius law above the dynamic crossover temperature. Qualitatively similar results were obtained in simulations of the two-dimensional (2D) version of the random-site model.[10,16] In previous work on the three-dimensional (3D) model using the nonlocal dynamics described above a power-law divergence of the relaxation time was reported at the transition temperature T_c.[11] In our case this temperature T_c is of the same order as the dynamic crossover temperature T_g for which our samples stay out of equilibrium during the entire simulation time. Therefore, we have no access to the equilibrium critical dynamics of the model.

B. $T<T_g$

This is the region in which nonequilibrium slow relaxation and aging are observed. Aging effects can be quantified

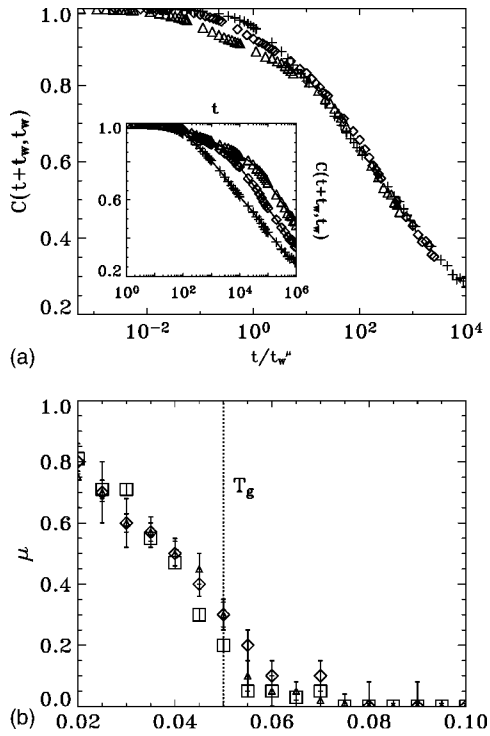

FIG. 3. Characterization of aging for $T<T_g$. (a) Autocorrelation functions $C(t+t_w,t_w)$ vs the rescaled time variable t/t_w^{μ} at $T=0.030<T_g$. The waiting times are $t_w=10^3$ (+), $t_w=10^4$ ($\diamond$), and $t_w=10^5$ ($\triangle$). The inset shows the same data represented as a function of time. (b) Temperature dependence of the aging exponent μ for different system sizes $N=L^3$ with $L=10$ ($\square$), $L=8$ ($\triangle$), and $L=6$ ($\diamond$).

by performing a nonstationary scaling analysis of the two time-autocorrelation functions. Experimental data in glasses are often analyzed in terms of the scaling form[17,18]

$$C(t+t_w,t_w) \approx F\left(\frac{h(t+t_w)}{h(t_w)}\right), \tag{5}$$

where $h(u)$ is known as the time-reparametrization function. A commonly used form is $h(u)=\exp(u^{1-\mu}/(1-\mu))$. Since this form implies an effective time scale growing with t_w as $\sim t_w^{\mu}$ we shall analyze our data in terms of the simpler expression

$$C(t+t_w,t_w) \approx F(t/t_w^{\mu}). \tag{6}$$

Figure 3(a) illustrates the procedure for $T=0.03$. The inset to the figure shows $C(t+t_w,t_w)$ as a function of t for three waiting times; $t_w=10^3, 10^4$, and 10^5. The main figure presents the same data plotted as a function of t/t_w^{μ} with $\mu \sim 0.7$, the value for which the collapse of the data at large times t is the best. Repeating this procedure for several different temperatures we obtained the T dependence of the aging exponent shown in Fig. 3(b). We find subaging behavior at low temperatures ($\mu \leqslant 1$) in the range $T<T_g$. When $T \to T_g$ μ decreases steeply to a value close to zero meaning that aging effects become negligible for $T>T_g \sim 0.05$. The figure also shows the size dependence of the aging exponent. It can also be seen that when the linear size of the system increases from $L=6$ to $L=10$ the decay of μ near $T_g \sim T_c$ becomes steeper. This makes it plausible that μ vanishes (and aging stops) right at the glass transition temperature T_c. Confirmation of this hypothesis would require a more detailed analysis of the L dependence of our results.

IV. ELECTRON DIFFUSION

The local charge correlation function discussed in the previous section does not provide direct information on the dynamics of current fluctuations in the medium. Information on this essential aspect of the physics of the Coulomb glass may be obtained from an analysis of carrier diffusion.

Let $\mathbf{r}_i(t)=(x_i(t),y_i(t),z_i(t))$ denote the position vector of an electron at time t, where x_i, y_i, and $z_i(t)$ are its coordinates before they are folded back into the simulation cell. We then have

$$\mathbf{r}_i(t) = \mathbf{r}_i(0) + \sum_{k=0}^{N_i(t)} \delta\mathbf{r}_i(k), \tag{7}$$

where $\mathbf{r}_i(0)$ is the electron's initial position, $N_i(t)$ is the total number of hops that it performed up to time t, and $\delta\mathbf{r}_i(k)$ is the displacement associated with the kth accepted move.

The mean-squared displacement between times t_w and $t+t_w$ is defined as

$$\Delta(t+t_w,t_w) = \frac{1}{M}\sum_{i=1}^{M} \langle \Delta x_i^2(t+t_w,t_w)\rangle, \tag{8}$$

where

$$\Delta x_i^2(t+t_w,t_w) = \frac{[\mathbf{r}_i(t+t_w)-\mathbf{r}_i(t_w)]^2}{3}, \tag{9}$$

and the angular brackets denote as before an average over realizations of the disorder, initial conditions, and the thermal histories.

Figure 4 shows the t dependence of $\Delta(t+t_w,t_w)$ for three values of the waiting time: $t_w=10^3, 10^4$, and 10^5. Data are displayed for two temperatures: $T=0.03<T_g$ [Fig. 4(a)] and $T=0.06>T_g$ [Fig. 4(b)].

It can be seen that $\Delta(t+t_w,t_w)$ is time-translational invariant for the higher temperature but exhibits aging for the lower one. Moreover, we observe that in the equilibrium regime $T>T_g$ the average motion is diffusive, $\Delta(t+t_w,t_w) \equiv \Delta(t) \propto t$, while this is not the case in the aging regime $T<T_g$.

We first discuss the case of high temperatures. In this case we can define a diffusion constant through $\Delta(t+t_w,t_w)=D(T)t$. We attempted to fit our results using the stretched-exponential expression $D(T) \sim \exp[-(T_1/T)^{\beta}]$. Using this form, a plot of $T^{\beta}\ln D^{-1}$ as a function of T should result in a horizontal line. The inset to Fig. 5(a) shows that this is indeed obtained for $\beta \sim 1$. The figure also shows the result of a similar plot using the value $\beta=0.5$ expected from the Efros-Shklovski variable range hopping law. It is apparent that our data cannot be described with this value of β. Similar deviations from the Efros-Shklovski law were also found in the

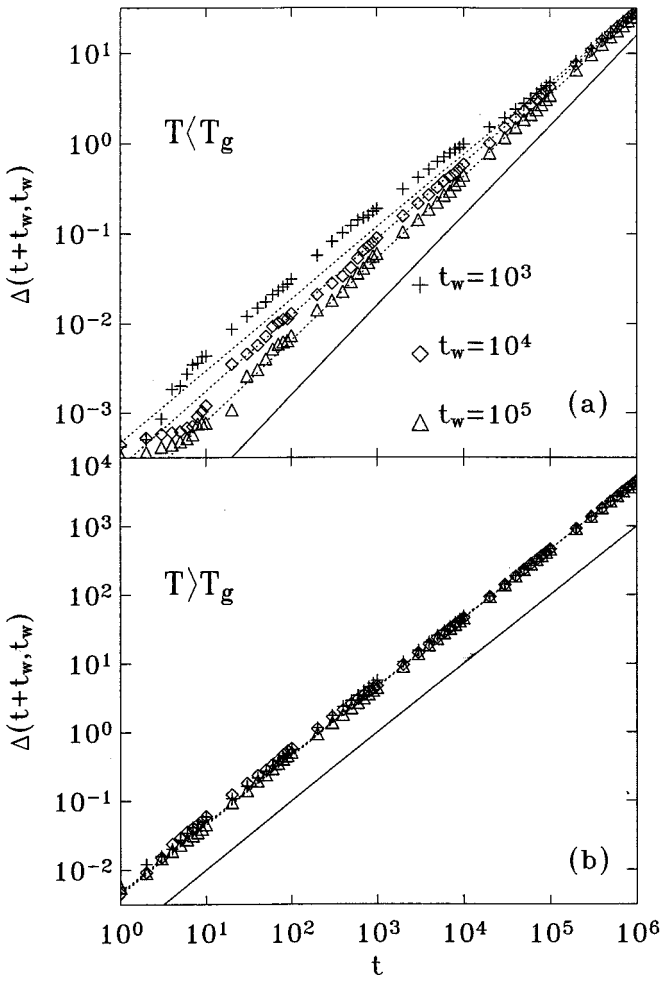

FIG. 4. Mean-squared displacement $\Delta(t+t_w,t_w)$ as a function of t for $t_w=10^3$ (+), $t_w=10^4$ ($\diamond$), and $t_w=10^5$ ($\triangle$). The solid line is the diffusion limit, $\Delta \propto t$: (a) $T=0.03<T_g$. The dotted lines are fits of the data to Eq. (10) over the last decade, $10^5<t<10^6$: (b) $T=0.06>T_g$.

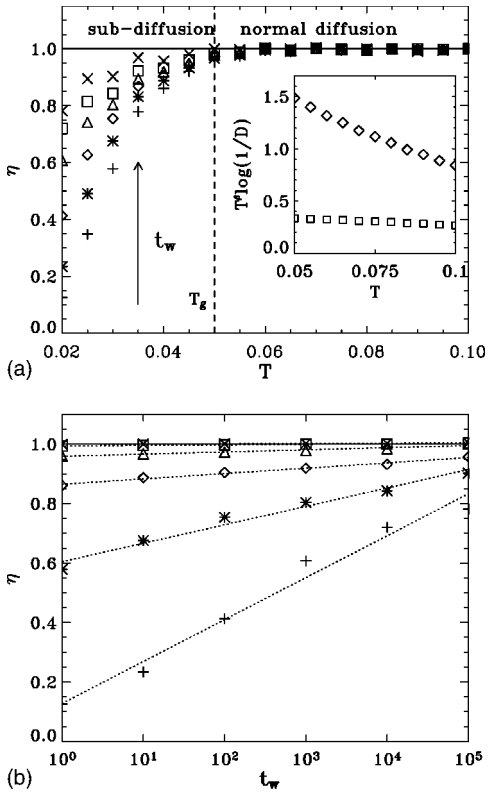

FIG. 5. (a) T dependence of the diffusion exponent η for $t_w=10^0$ (+), $t_w=10^1$ (*), $t_w=10^2$ ($\diamond$), $t_w=10^3$ ($\triangle$), $t_w=10^4$ ($\square$), and $t_w=10^5$ ($\times$) from bottom to top. The dashed line indicates the crossover temperature T_g. (Inset): T dependence of the diffusion constant D in the equilibrium regime, $T>T_g$. We plot $T^{\beta}\log D^{-1}$ as a function of T for $\beta=1$ ($\square$) and $\beta=0.5$ ($\diamond$). (b) Waiting-time dependence of η for $T=0.02$ (+), $T=0.03$ (*), $T=0.04$ ($\diamond$), $T=0.05$ ($\triangle$), $T=0.06$ ($\square$), and $T=0.07$ ($\times$).

2D version of the model[15,27] for which we found $\beta \approx 3/4$.[27]

We now turn to the analysis of the low-temperature results. In this case the time dependence of Δ cannot be described by a simple power law but we can still characterize the diffusion in this regime by fitting the t dependence of $\Delta(t+t_w,t_w)$ for our longest times (the last decade in t, for example) to an expression of the form

$$\Delta(t+t_w,t_w) \sim t^{\eta(t_w,T)}. \tag{10}$$

Equation (10) defines an effective diffusion exponent η that depends on both the waiting time and the temperature. The asymptotic fits for $T=0.03$ are represented by the dotted lines in Fig. 4(a) where the normal diffusion limit $\eta=1$ is also shown for comparison.

Figure 5 summarizes our results for the diffusion exponent in the aging region. The temperature dependence of η for several values of t_w is shown in Fig. 5(a). It can be seen that in the equilibrium regime, $T>T_g$, $\eta=1$ for all t_w and T. Below T_g, however, the diffusion exponent decreases with decreasing temperature for all values of t_w, reflecting that electron motion becomes increasingly sluggish.

The dependence of η with t_w at fixed T is shown in Fig. 5(b) for several temperatures. The exponent η increases with t_w, eventually reaching the diffusion limit $\eta=1$ for long waiting times. At low temperature this variation is slow (approximately logarithmic). This is yet another manifestation of the slow relaxation that characterizes the glassy phase of the Coulomb glass.

The characterization of diffusion through a diffusion exponent is familiar in the study of random walks in random media where one generally finds subdiffusive behavior ($\eta<1$) in those physical situations in which the distribution of the time intervals between successive hops of the diffusing particle has sufficiently long tails that the central limit theorem no longer holds.[28] It would be interesting to examine the distribution of these times in the aging regime of our system.

V. HETEROGENEOUS DYNAMICS

To establish a relationship between the observed aging effects and the microscopic motion of electrons we analyzed the evolution of the diffusion front. This latter is defined through the probability density of the squared displacements:

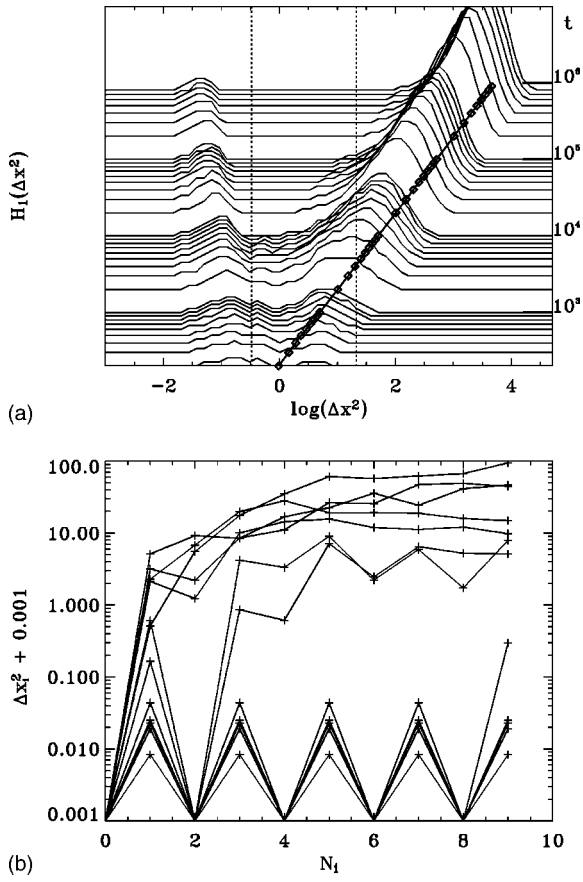

FIG. 6. (a) Evolution of the diffusion front $H_1(\Delta x^2)$ for $t_w = 10^6$ and $T=0.060$. Histograms are scaled and shifted vertically by an amount $\log(t)$ so that their baselines coincide with the time they correspond to. The symbols ($\diamond$) represent the mean-squared displacement $\Delta(t+t_w,t_w)$. The vertical lines are located at the positions a_0^2 and L^2, where a_0 is the mean distance between sites and $L=10$ the linear size of the system. (b) Typical squared displacements of a selected set of electrons as a function of hop number. The temperature is $T=0.060$. We show the first ten hops after $t_w=10^6$ steps. The selected graphs illustrate typical dipolar and diffusive electron trajectories.

$$H_1(\Delta x^2,t,t_w) = \frac{1}{M}\sum_i \langle \delta(\Delta x^2 - \Delta x_i^2(t+t_w,t))\rangle, \qquad (11)$$

where $\delta(x)$ is the usual δ function. It is easy to show that for a stationary and homogeneous diffusion process the above distribution takes the form

$$H_1^{\mathrm{diff}}(\Delta x^2,t) = \Phi\left(\frac{\Delta x^2}{Dt} - 1\right), \qquad (12)$$

where $\Phi(x)$ is approximately Gaussian. H_1^{diff} thus exhibits a single peak whose position increases linearly with time. To compute H_1 from our numerical data we must appropriately coarse grain the variable Δx^2. Since we found that the distribution of electron squared displacements is very broad we chose a regular coarse graining in $\log(\Delta x^2)$. In Fig. 6(a) we show the evolution of the computed $H_1(\Delta x^2,t,t_w)$ as a function of $\log(\Delta x^2)$ for $t_w=10^6$ and $T=0.060>T_g$. For this value of the temperature H_1 is independent of the waiting time if t_w is large enough. This is consistent with the observed time translation invariance of the charge autocorrelation functions and the mean squared displacement at this temperature. The histograms shown in the figure were scaled conveniently and shifted vertically by an amount $\log(t)$ to make their baselines coincide with the time they correspond to.

Note that the diffusion front, located initially at $\Delta x^2=0$, splits rapidly into two peaks. The position of the first peak is almost time independent at long times. This peak corresponds to squared displacements smaller than the average impurity distance a_0. The center of the second peak increases linearly with time and its location coincides with the mean squared displacements at long times. The interpretation of these results is that the electron dynamics is heterogeneous and characterized by the existence of two dynamical modes that can be clearly distinguished: (a) the diffusive mode—electron motion is unbound and diffusive; it corresponds to metallic hopping as found in Ref. 10 and (b) the confined mode—electrons remain confined within small regions of space during the observation time.

Examples of trajectories of electrons of these two types are shown in Fig. 6(b) at the same temperature and for the same waiting time as above. The displacements are represented as a function of the hop number N_i. We only show the ten first hops after a waiting time $t_w=10^6$.

Some of the trajectories correspond to electrons that hop back and forth between two sites. Δx^2 then oscillates between 0 and b_i^2, the distance between the sites involved in the motion. This fluctuating dipolar motion contributes to most of the weight of the first peak in the histograms of Fig. 6(a). It is important to note that, although this fluctuating motion appears regular when plotted as a function N_i, it is in fact extremely irregular when viewed as a function of time, since the time intervals between successive jumps are very widely distributed. The rest of the trajectories shown in Fig. 6(b) are those of diffusive electrons that contribute to the metallic peak in the histograms of Fig. 6(a).

We turn now to the analysis of the statistics of hopping rates which is important to understand the source of spontaneous fluctuations in the system. To this end we consider the joint distribution function

$$H_2(\Delta x^2,n_h;t,t_w) = \sum_i \langle \delta(\Delta x_i^2(t+t_w,t_w) - \Delta x^2) \times \delta(n_i(t,t_w) - n_h)\rangle, \qquad (13)$$

where $n_i = N_i/\overline{N_h}$ is the number of hops of an electron i normalized by $\overline{N_h}=\Sigma_i N_i/M$, the average number of hops per electron.

We use a regular coarse graining in $\log(\Delta x^2)$ and n_h to compute the corresponding histograms. These are displayed in Figs. 7(a) and 7(b) for $T=0.070>T_g$ and $T=0.040<T_g$, respectively. Both plots correspond to $t=t_w=10^6$.

The two dynamical modes described above can be easily identified in the equilibrium situation [Fig. 7(a)]. The single peak at large Δx^2 corresponds to the diffusive mode while the two ridges at low values of Δx^2 correspond to the dipolar mode. Note that the hopping rates of electrons involved in

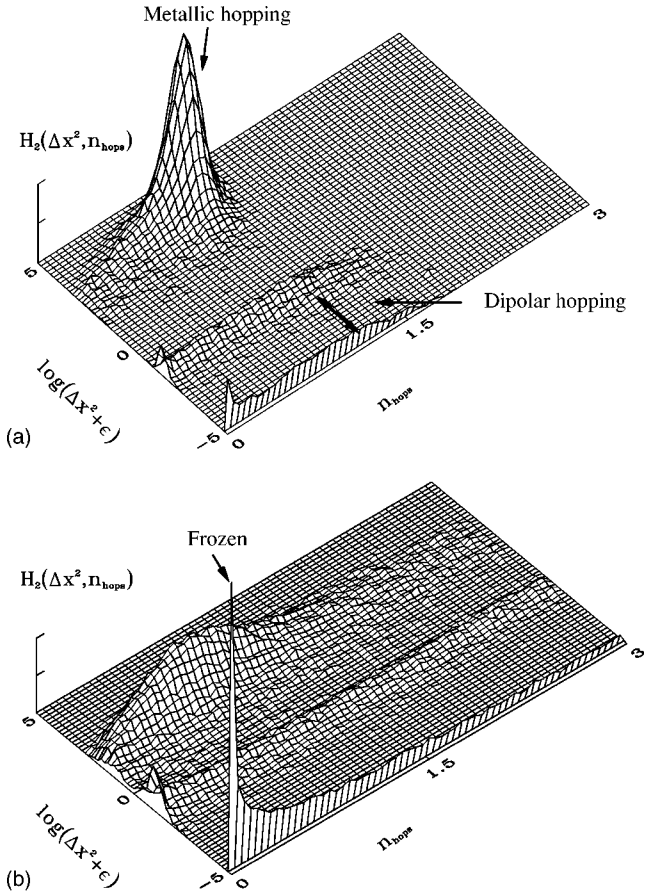

FIG. 7. The joint probability distribution of squared displacement Δx^2 and normalized hopping rates $H_2(\Delta x^2, n_h)$ for $T=0.07$ (a) and $T=0.04$ (b). The histograms are taken at time $t=10^6$ after a waiting time $t_w=10^6$.

dipolar motion have a much wider distribution than those of diffusive electrons.

Figure 7(b) shows that the two modes are still distinguishable at low temperatures, when the system is out of equilibrium. The structure of the modes is qualitatively different, however. Not only the distribution of hopping rates is now much broader but a small fraction of electrons with low hopping rate lies inbetween the two modes. The presence of these electrons, which cannot be clearly associated with any of the modes, suggests that a very slow exchange of carriers between them may take place in the course of the relaxation. We shall further discuss this issue below.

To explore in more detail the properties of electrons contributing to each of these modes we found it convenient to define for each electron the variable

$$d_i(t_w) = \frac{1}{t}\sum_{\tau=1}^{t} \frac{\Delta x_i^2(\tau + t_w, t_w)}{\tau}. \tag{14}$$

This quantity characterizes the mobility of the electron during a time interval of length t after t_w. For a carrier that diffuses normally in this time span with a diffusion constant D, $d_i \sim D$. For an electron that remained confined in a region of linear size a during this time interval, $d_i \sim a^2 \ln(t)/t$. Finally, for a frozen electron, i.e., one that did not move at all in the time interval under consideration, $d_i=0$.

We study the probability density of d defined as

$$f(d, t_w) = \frac{1}{M}\sum_{i=1}^{M} \langle \delta(d_i - d)\rangle. \tag{15}$$

As discussed above we expect $f(d, t_w)$ to exhibit two well separated peaks: one at $d=D(t_w)$, the average diffusion constant of the diffusing electrons at time scale t_w and the other at $d=a(t_w)^2 \ln(t)/t$, where $a(t_w)$ is the typical size of the regions of confined motion at the same time scale. The width of the peaks gives the dispersion of these quantities.

We also introduce the cumulative distribution function

$$F(d, t_w) = \int_0^d f(x, t_w) dx. \tag{16}$$

Results are displayed in Fig. 8 where we plot $f(d, t_w)$, and its cumulative distribution function for three temperatures, $T=0.02<T_g$, $T=0.035<T_g$, and $T=0.060>T_g$ and waiting times $t_w=10^n$ with $n=0,1,2,3,4,5$, and 6. In all cases we see the appearance of the two peaks referred to above. The distributions are stationary for $T>T_g$ for which the system equilibrates rapidly but they show aging in the nonequilibrium regime.

A striking feature of the function f in the aging regime [cf. Figs. 8(a) and 8(c)] is that the positions of the peaks are almost independent of t_w. This means that the diffusion constant of the "metallic" electrons is time independent. The height of the peaks, however, does depend on time scale: as time elapses from the quench, the proportion of diffusing carriers diminishes while that of the confined ones increases. This is a direct manifestation of the exchange mechanism that we hinted at above. The fact that the location of the peaks is only weakly dependent on t_w indicates that the effective mobility of the diffusive electrons is not much affected by the slow changes of the environment that result from the aging process.

The plateaus that appear in the corresponding cumulative distribution functions right after the peaks [cf. Figs. 8(b), 8(d), and 8(f)] can be used to measure the relative populations of the modes. We see a first plateau corresponding to the area of $f(d, t_w)$ below the dipolar peak and a second plateau corresponding to the additional area below the metallic peak. It can be seen that the cumulative distribution function does not saturate to unity at low temperatures [cf. Figs. 8(b) and 8(d)] while it does at high temperatures [cf. Fig. 8(f)]. The difference is due to the fact that, at low temperature, a fraction of the electrons remain frozen during the observation time. These were not counted in the numerical evaluation of the integral in Eq. (16). Another manifestation of the presence of frozen carriers is the pronounced asymmetry of the two lower ridges in the lower panel of Fig. 7 in the zero hopping-rate limit.

We can now use the height of the plateaus in Figs. 8(b), 8(d), and 8(f) to measure the populations of the different modes. These are represented as a function of temperature for $t_w=10^6$ in Fig. 9(a). It is seen that the proportion of

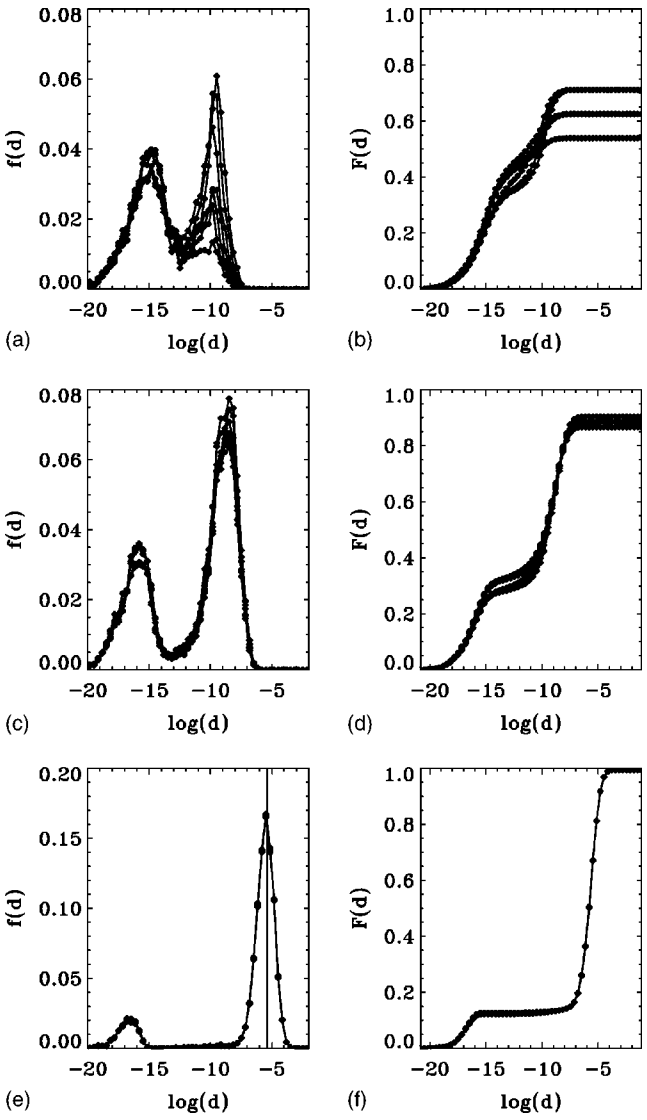

FIG. 8. Probability density $f(d)$ (left panels) and the corresponding distribution function $F(d)$ (right panels) for three temperatures, $T=0.02$ (a), (b), $T=0.035$ (c), (d), and $T=0.06$ (e), (f). In all cases $t=10^6$ and the waiting times are $t_w=10^n$ with $n=0,1,2,3,4,5,$ and 6. The solid line in (e) indicates the location of the diffusion constant $D(T)$ calculated from the mean-squared displacements of electrons at $T=0.060$.

diffusive electrons increases with increasing temperature while, at the same time, that of dipolar and frozen ones decreases. Note that a crossover between the regime dominated by diffusive electrons and that dominated by confined ones is located precisely at T_g.

The waiting-time dependence of the populations is shown in Fig. 9(b) for two temperatures: $T=0.03<T_g$ (left panel) and $T=0.06>T_g$ (right panel). These populations are time independent at the highest temperature but vary logarithmically with time in the aging regime.

It is quite tempting to try to relate these observations to the relaxational properties of the conductivity. Assuming that the Einstein relation holds in the nonequilibrium regime, the conductivity at scale t is $\sigma \propto n \int dD f(D,t)$, where n is the electron density and the integral extends over the diffusive

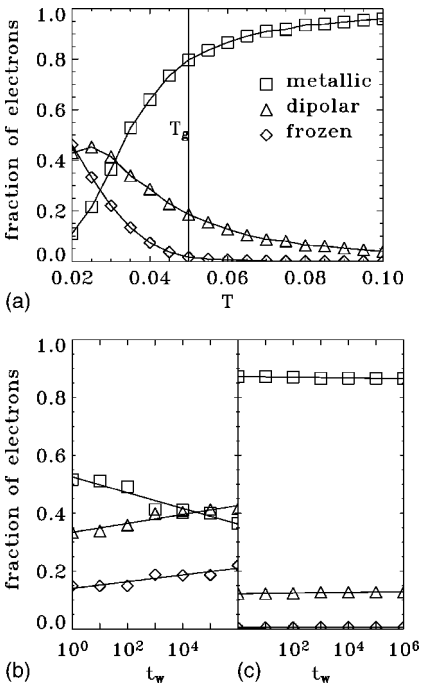

FIG. 9. (a) Density of diffusive (□), confined (△), and frozen electrons (◇) during time scale $t=10^6$ as a function of the temperature. Waiting time is $t_w=10^5$. The line indicates the location of the crossover temperature T_g. (b), (c) Waiting-time dependence of the same densities for $T=0.03<T_g$ (b) and $T=0.06>T_g$ (c). The meaning of the symbols is the same as in (a).

peak. We saw earlier that the position of the peak $\bar{D}$ is time independent. This implies $\sigma \sim n p_D \bar{D}$, where p_D is the fraction of diffusing carriers. Since the latter decreases logarithmically with time, this simple argument predicts logarithmic relaxation of the conductivity which is one of the main experimental observations. Whether the assumptions leading to this result are valid has to await direct computation of the current in the aging regime, in the presence of an applied electric field.[27]

VI. CONCLUSIONS

We have studied the relaxational properties of the three-dimensional random-site Coulomb glass model after a quench from high temperature. We found a crossover from stationary to slow nonstationary dynamics at a temperature T_g that is very close to T_c, the equilibrium glass transition temperature of the model. This crossover can be seen even in relatively small samples because of the exponential increase of the equilibration time with decreasing temperature.

We found that at low temperature the dynamics of local charge fluctuations and that of current fluctuations show aging. In the former case, the relaxation obeys simple scaling laws characterized by a temperature-dependent aging exponent $\mu(T)$. Analysis of the temperature and system-size dependence of $\mu(T)$ suggests that in the thermodynamic limit the observed crossover at $T_g \sim T_c$ becomes a real dynamic transition that occurs precisely at T_c.

The analysis of the properties of diffusion fronts revealed that the dynamics of carriers is heterogeneous as it was found in other glassy systems.[21] We found that for each time scale two classes of electrons may be identified: those that have diffusive motion during the observation time and those whose motion in the same time interval remains confined. Only electrons belonging to the former class contribute to the dc conductivity while the others only contribute to the dielectric screening.

In the region of low temperatures where aging is observed electrons are slowly exchanged between these two modes with the consequence that the population of metallic electrons decreases logarithmically with time without appreciable change of the their diffusion constant. This provides a plausible explanation for the logarithmic relaxation of the conductance after a quench that was observed experimentally.

We believe that the local microscopic dynamics used here, which is a realistic description of hopping processes in experimental systems, plays an important role in the phenomena that we observed. This type of dynamics favors the appearance of local effective constraints that relate our model to kinetically constrained models in which slow dynamics arises from restrictions on the allowed transitions between configurations.

ACKNOWLEDGMENTS

We thank Z. Ovadyahu, L. F. Cugliandolo, J. Kurchan, and T. Giamarchi for valuable discussions. We also acknowledge financial support from the Argentina-Francia cooperation SECYT-ECOS, Project No. A01E01. A.B.K. and D.D. acknowledge support from Conicet, CNEA, ANPCyT (Grant No. PICT99-03-06343) and Fundación Antorchas (Proy. 14116-147). A.B.K. also acknowledges support of a grant from the Swiss National Science Foundation.

[1] M. Ben-Chorin, Z. Ovadyahu, and M. Pollak, Phys. Rev. B **48**, 15 025 (1993); Z. Ovadyahu and M. Pollak, Phys. Rev. Lett. **79**, 459 (1997).

[2] G. Martinez-Arizala, C. Christiansen, D. E. Grupp, N. Markovic, A. M. Mack, and A. M. Goldman, Phys. Rev. B **57**, R670 (1998).

[3] A. Vaknin, Z. Ovadyahu, and M. Pollak, Phys. Rev. Lett. **84**, 3402 (2000); Phys. Rev. B **65**, 134208 (2002).

[4] A. Vaknin, Z. Ovadyahu, and M. Pollak, Phys. Rev. Lett. **81**, 669 (1998).

[5] V. Orlyanchik and Z. Ovadyahu, Phys. Rev. Lett. **92**, 066801 (2004).

[6] B. I. Schklovskii and A. L. Efros, *Electronic Properties of Doped Semiconductors* (Springer, Berlin, 1984).

[7] *Electron-Electron Interactions in Disorder Systems*, edited by A. L. Efros and M. Pollak (North-Holland, Amsterdam, 1985).

[8] M. Pollak, Philos. Mag. B **50**, 265 (1984); M. Grünewald *et al.*, J. Phys. C **15**, L1153 (1982).

[9] J. H. Davies, P. A. Lee, and T. M. Rice, Phys. Rev. Lett. **49**, 758 (1982); Phys. Rev. B **29**, 4260 (1984).

[10] W. Xue and P. A. Lee, Phys. Rev. B **38**, 9093 (1988).

[11] E. R. Grannan and Clare C. Yu, Phys. Rev. Lett. **71**, 3335 (1993).

[12] For recent developments see M. Mueller and L. B. Ioffe, cond-mat/0406324 (unpublished); S. Pankov and V. Dobrosavljevic, cond-mat/0406406 (unpublished).

[13] A. Pérez-Garrido, M. Ortuño, A. Díaz-Sánchez, and E. Cuevas, Phys. Rev. B **59**, 5328 (1999).

[14] C. C. Yu, Phys. Rev. Lett. **82**, 4074 (1999).

[15] D. N. Tsigankov *et al.*, Phys. Rev. B **68**, 184205 (2003).

[16] D. R. Grempel, Europhys. Lett. **66**, 854 (2004).

[17] L. C. E. Struik, *Physical Aging in Amorphous Polymers and Other Materials* (Elsevier, Amsterdam, 1978).

[18] E. Vincent *et al.*, in *Complex Behavior of Glassy Systems*, edited by M. Rubi and C. Perez-Vicente (Springer, Berlin, 1997).

[19] J. P. Bouchaud, L. F. Cugliandolo, and J. Kurchan, in *Spin Glasses and Random Fields*, edited by A. P. Young (World Scientific, Singapore, 1997); L. F. Cugliandolo, in *Slow Relaxation and Nonequilibrium Dynamics in Condensed Matter*, Les Houches Session 77, 2002 (unpublished); J. L. Barrat, J. Dalibard, J. Kurchan, M. V. Feigel'man, cond-mat/0210312 (unpublished).

[20] L. F. Cugliandolo and J. Kurchan, Phys. Rev. Lett. **71**, 173 (1993); J. Phys. A **27**, 5749 (1994).

[21] J. P. Garrahan and D. Chandler, Phys. Rev. Lett. **89**, 035704 (2002); L. Berthier and J. P. Garrahan, Phys. Rev. E **68**, 041201 (2003); S. Whitelam, L. Berthier, and J. P. Garrahan, Phys. Rev. Lett. **92**, 185705 (2004).

[22] H. E. Castillo, C. Chamon, L. F. Cugliandolo, J. L. Iguain, and M. P. Kennett, Phys. Rev. B **68**, 134442 (2003).

[23] F. Ritort and P. Sollich, Adv. Phys. **52**, 219 (2003).

[24] B. I. Shklovskii, Phys. Rev. B **67**, 045201 (2003).

[25] K. Shtengel and C. C. Yu, Phys. Rev. B **67**, 165106 (2003).

[26] T. Vojta and M. Schreiber, Phys. Rev. Lett. **73**, 2933 (1994); E. R. Grannan and C. C. Yu, *ibid.* **73**, 2934 (1994); A. Díaz-Sánchez, M. O. Ortuño, A. Pérez-Garrido, and E. Cuevas, Phys. Status Solidi B **218**, 11 (2000).

[27] A. B. Kolton, D. Grempel, and D. Domínguez (unpublished).

[28] J. P. Bouchaud and A. Georges, Phys. Rep. **195**, 127 (1990).